Available online at www.sciencedirect.com
ScienceDirect
Computer Physics Communications 178 (2008) 635–646
Computer Physics Communications
www.elsevier.com/locate/cpc

Structural reinforcement in a spring-block model of stress-induced fracture propagation

G.A. Esleta, C. Monterola *

National Institute of Physics, University of the Philippines, Diliman 1101, Quezon City, Philippines

Received 20 February 2007; received in revised form 8 December 2007; accepted 11 December 2007
Available online 23 December 2007

Abstract

We present a mechanism-based model of fracture propagation in a two-dimensional elastic sheet subjected to biaxial stretching. The time evolution of lattice stretching is formulated using a set of coupled nonlinear differential equations describing the network dynamics of masses connected by springs. We show that reinforcement based on a Gaussian spatial distribution of failure thresholds is effective in hindering tear propagation, that is, it delays the onset of breakage and reduces the total fractured sites at equilibrium time. The method presented here is general—it can incorporate any type of load distribution and test any reinforcement procedures.

PACS: 83.60.Uv; 04.60.Nc; 02.60.-x; 83.85.St

Keywords: Fracture propagation; Fragmentation; Discrete element modeling; Reinforcement; Lattice models

1. Introduction

Material fracture and fragmentation are ubiquitous in nature. They are observed on a broad range of length scales from geological phenomena such as earthquakes, to industrial processes and applications, down to the break-up of macromolecules and heavy nuclei. These phenomena may be considered universal in a sense that they may occur under a variety of conditions and in many types of materials.

Understanding how materials fracture is a fundamental scientific and technological problem which can have an enormous industrial and social impact. In materials science and engineering, for instance, modeling the dynamics of fracture propagation aids in the design of better materials and refines the quality of preexisting structures. In geology, crack propagation models of earthquakes allow better prediction and mitigation of large-scale destruction.

Even until now, a profound understanding is still lacking of phenomena such as how cracks nucleate, the formation of crack networks and the resulting size distribution of fragments, the dynamics of crack propagation, and the collective behavior of many interacting cracks. There have been attempts to study fragmentation using analytical approaches [1], but these are limited and scarce due to the complexity of multi-crack interactions. Thus, probing crack dynamics mainly rely on numerical simulations using simple dynamical models.

In engineering, standard continuum finite element models are used for modeling progressive damage evolution in homogeneous, quasi-brittle materials [2]. First developed by R. Courant in 1943, finite element analysis (FEA) has become indispensable in the structural and fatigue analysis of materials. It has become a solution to the task of predicting structural failure by showing trouble spots in a material and allowing designers to see the theoretical stresses and strains within. It can also help designers to predict the lifespan of a material or structure by showing the effects of cyclic loading.

An electrical analog of the fracture of solid materials is the Random Fuse Model (RFM), where one considers a triangular lattice with fuses with identical conductances and random breaking thresholds t [3]. A fuse burns irreversibly when the current passing through it exceeds its designated threshold t. Each time a fuse is burnt, it is necessary to re-calculate the

* Corresponding author. Tel.: (+632) 9818500, loc. 3703; fax: (+632) 9280286.
E-mail address: cmonterola@nip.upd.edu.ph (C. Monterola).

0010-4655/$ – see front matter
doi:10.1016/j.cpc.2007.12.003

current redistribution in the lattice to determine the subsequent breaking of a fuse. The process of breaking of a fuse, one at a time, is repeated until the lattice system fails completely, producing an irregular fracture surface.

The most common approach to fracture, however, is based on numerical simulation of lattice models. Also known as discrete element modeling, the use of lattice models began in 1967, when Burridge and Knopoff [4] introduced a one-dimensional system of blocks and springs to study the role of friction along a fault in the propagation of an earthquake. Since then, similar dynamical models of many-body systems have been investigated, ranging from propagation and rupture in earthquakes [5,6], to the fractures of overlayers on a rough substrate [7,8], and even to the breakup of eggshells due to impact or explosion [9].

In this paper a theoretical study of the fracture and fragmentation of an elastic sheet, such as woven fabrics, due to biaxial stretching is presented. The sheet is modeled using a regular two-dimensional (2D) network of masses and springs. The full nonlinear equations for the forces are derived in terms of displacements, and used them to follow the time evolution of the system as it undergoes biaxial stretching. We then performed structural reinforcement of the lattice by (a) increasing the failure thresholds along cracks and weak spots, and (b) varying the distribution of failure thresholds. Our results demonstrated that a simple Gaussian spatial distribution of failure thresholds is most effective and most efficient in impeding tear propagation.

2. Model

Our proposed model for surface fracture is defined on a regular L by L square lattice with spacing a as shown in Fig. 1. The lattice sites, labeled by (i, j) where $1 \leqslant i, j \leqslant L$, represent point-like material elements with identical masses m. In woven fabric modeling, these nodes represent the interlacing or knits between threads. For simplicity and ease of computation, the displacement of the (i, j)th mass is restricted to two dimensions $x_{i,j}$ and $y_{i,j}$.

To model the elasticity of the material, neighboring masses are connected by linear elastic springs with identical stiffness κ and unstretched lengths l_0, chosen to be equal to the lattice spacing a. Following the work of Olami et al. [10], free boundary conditions (FBC) are imposed, in which the sites on the lattice edges have three neighbors each while those at the corners have two.

2.1. Tearing dynamics

In order to account for tear propagation in the model, a spring breaks when its length exceeds its designated failure threshold $l_{\max}$, from which point on it exerts no force. In the simulations, tearing is implemented by setting the stiffness κ of the spring to zero. The elastic force is then released on the broken spring and redistributed to neighboring springs. If after some iterations the neighboring springs exceed their threshold value due to the additional force, they also fail. Successive spring failures result to crack nucleation, growth, and may ultimately lead to the complete breakup of the material.

External load is imposed on the lattice by adding a constant outward force $F_{\text{ext}}(t) \equiv F_{\text{ext}}$ at the edges. This type of loading simulates biaxial stretching (i.e., stretching along both horizontal and vertical directions), which is applicable to certain materials like textiles and woven fabrics. After prescribing the initial conditions of a specific reinforcement procedure studied, the time evolution of the lattice is followed by solving the equation of motion of the nodes. Following the work of Leung et al. [6], the set of second-order coupled differential equations describing the spatial motion of the springs are:

$$m\ddot{\vec{r}}_{i,j} = \vec{F}_{i,j}, \quad 1 \leqslant i, j \leqslant L, \tag{1}$$

where $\vec{r}_{i,j} \equiv x_{i,j}\hat{e}_i + y_{i,j}\hat{e}_j$.

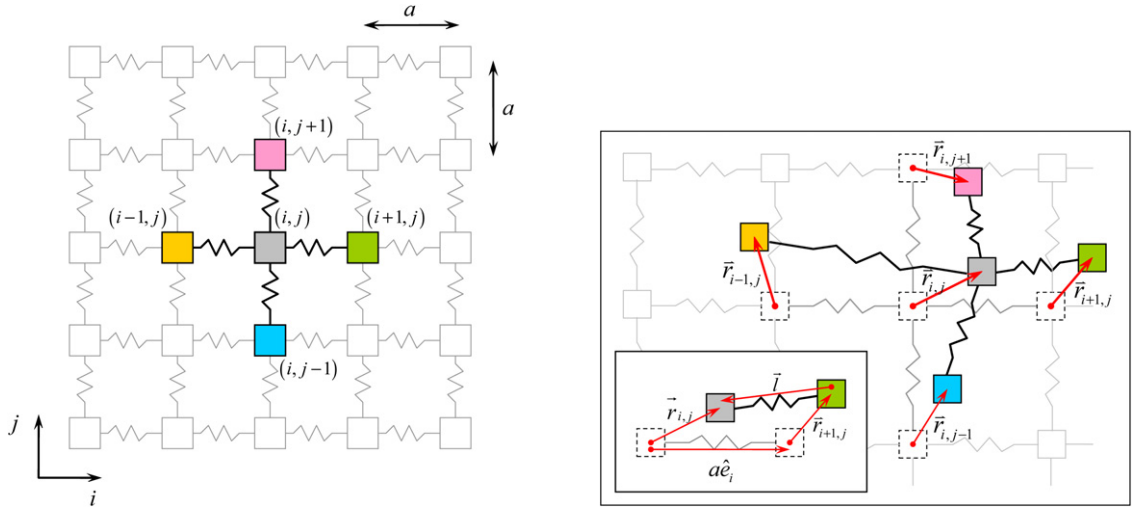

(a) (b)

Fig. 1. (a) Model architecture and index conventions. The lattice sites represent point-like material elements with identical masses m. Neighboring masses are connected by linear elastic springs with rest lengths $l_0 \equiv a$ and stiffness κ. Free boundary conditions (FBC) are used, with three neighbors at the edges and two at corners. (b) Body diagram for the (i, j)th node and its four nearest neighbors.

The vector $\vec{F}_{i,j} \equiv F^x_{i,j}\hat{e}_i + F^y_{i,j}\hat{e}_j$ is the total force acting on (i, j) and is given by

$$\vec{F}_{i,j} = \vec{f}_{L(i,j)} + \vec{f}_{(i,j+1)-(i,j)} + \vec{f}_{(i-1,j)-(i,j)} + \vec{f}_{(i+1,j)-(i,j)} + \vec{f}_{(i,j-1)-(i,j)}, \quad (2)$$

where $\vec{f}_{(i\pm1,j\pm1)-(i,j)}$ is the force exerted by a neighboring block on (i, j), and $\vec{f}_{L(i,j)}$ the external loading force. It is important to note that $\vec{f}_{L(i,j)}$ has a value only at the lattice edges and is zero elsewhere:

$$\vec{f}_{L(i,j)} = \begin{cases} F_{\text{ext}}\hat{e}_j, & j = L \text{ (upper edge)}, \\ -F_{\text{ext}}\hat{e}_i, & i = 1 \text{ (left edge)}, \\ F_{\text{ext}}\hat{e}_i, & i = L \text{ (right edge)}, \\ -F_{\text{ext}}\hat{e}_j, & j = 1 \text{ (lower edge)}, \\ 0, & \text{elsewhere.} \end{cases} \quad (3)$$

To solve for the functional form of $\vec{f}_{(i+1,j)-(i,j)}$, we first define a *length vector* $\vec{l}_{(i+1,j)-(i,j)}$, which specifies the length and orientation of the spring connecting nodes (i, j) and $(i+1, j)$. By considering the geometry of the springs (Fig. 1(b)), $\vec{l}_{(i+1,j)-(i,j)}$ can be determined as

$$\vec{l}_{(i+1,j)-(i,j)} = (x_{i,j} - x_{i+1,j} - l_0)\hat{e}_i + (y_{i,j} - y_{i+1,j})\hat{e}_j. \quad (4)$$

Since the springs are linear, the force $\vec{f}_{(i+1,j)-(i,j)} \equiv f^x_{(i+1,j)-(i,j)}\hat{e}_i + f^y_{(i+1,j)-(i,j)}\hat{e}_j$ exerted by node $(i + 1, j)$ on (i, j) is defined by Hooke's Law:

$$f^x_{(i+1,j)-(i,j)} = -\kappa\left[1 - \frac{l_0}{\|\vec{l}_{(i+1,j)-(i,j)}\|}\right](x_{i,j} - x_{i+1,j} - l_0), \quad (5)$$

$$f^y_{(i+1,j)-(i,j)} = -\kappa\left[1 - \frac{l_0}{\|\vec{l}_{(i+1,j)-(i,j)}\|}\right](y_{i,j} - y_{i+1,j}). \quad (6)$$

Because of the symmetry of the system, $\vec{f}_{(i-1,j)-(i,j)}$, $\vec{f}_{(i,j+1)-(i,j)}$ and $\vec{f}_{(i,j-1)-(i,j)}$ can be easily obtained by switching variables and/or indices in Eqs. (5) and (6).

The equation of motion along the horizontal direction now takes the form

$$\begin{aligned} m\ddot{x}_{i,j} = f^x_{L(i,j)} - \kappa\Bigg\{&\left[1 - \frac{l_0}{\|\vec{l}_{(i,j+1)-(i,j)}\|}\right](x_{i,j} - x_{i,j+1}) \\ &- \left[1 - \frac{l_0}{\|\vec{l}_{(i-1,j)-(i,j)}\|}\right](x_{i-1,j} - x_{i,j} - l_0) \\ &+ \left[1 - \frac{l_0}{\|\vec{l}_{(i+1,j)-(i,j)}\|}\right](x_{i,j} - x_{i+1,j} - l_0) \\ &- \left[1 - \frac{l_0}{\|\vec{l}_{(i,j-1)-(i,j)}\|}\right](x_{i,j-1} - x_{i,j})\Bigg\}. \end{aligned} \quad (7)$$

Again, the equation of motion along the vertical direction follows by switching the variables and/or indices in Eq. (7).

3. Numerical simulations

As basis of comparison, we first consider the case where the lattice is homogeneous and unmodified, i.e., a fixed threshold value $l_{\max} \equiv 1.5l_0$ is set for all the springs. Simulations are performed over a wide range of values of the stretching force $0 < F_{\text{ext}} \leqslant 0.6$, using a lattice size $L = 24$. Without loss of generality, we choose our units such that $a = l_0 = 1$, $m = 1$, and $\kappa = 1$.

The nodes are at rest initially. An external load given by Eq. (3) is then introduced to the lattice, stretching the lattice in both directions. For all iterations, the fourth order Runge–Kutta Method (RK4) is used to solve the equations of motion given by Eq. (1), using a time step $\delta t = 2^{-10}$ ($\sim 1 \times 10^{-3}$) and an integration time $t_{\text{final}} = 300$. The value of t_{final} is arbitrarily chosen and can be set to any value for purpose of comparing lattice of different sizes as discussed in more detail in Section 5.

The discretization error in RK4 is in the order of $(\delta t)^5$ per time step application [11]. Since our method for an $N \times N$ lattice size involves solving $4N^2$ differential equations ($2N^2$ equations for the positions and $2N^2$ equations for the velocities), the total accumulated error $\delta\xi$ up to t_{final} is about $4N^2 t_{\text{final}}(\delta t)^4$, or rearranging $\delta t \sim (\delta\xi/4N^2 t_{\text{final}})^{1/4}$. To illustrate, if at $t_{\text{final}} = 300$ the desired upper error bound for both the position and velocity is less than 1% ($\delta\xi = 0.01$) for $N = 100$ then the largest possible δt is 0.005. Our choice of $\delta t \sim 1 \times 10^{-3}$ provides a $\delta\xi \sim 1.2 \times 10^{-5}$, and therefore, no time delay error on the onset of breakage bigger than δt ($l_{\max}\delta\xi \ll l_{\max}$) is expected.

The RK4 belongs to a one step method type of solving differential equations, i.e. the value of $\{y_{n+1}\}$ is completely determined by $\{y_n\}$, and as described above, discretization error is solely determined by δt. In contrast, a multistep method (like Adams–Bashfort, Adams–Moulton, Nyström, Milne–Simpson, etc.) requires the values of $\{y_n, y_{n-1}, \ldots, y_{n+1-k}\}$ to calculate $\{y_{n+1}\}$, and therefore convergence analysis of the interpolating polynomials that relates the previous time steps is necessary to approximate "continuum" features [11]. Although generally more accurate than one step methods, multistep methods are not suitable for the boundary conditions of the problem at hand.

The computational complexity of the RK4 method utilized here is proportional to N^2. A possible implementation improvement is achievable by using adaptive time steps or solving the $4N^2$ set of coupled differential equations via neural networks (NN). Previously, the complexity of NN differential equation solver is shown to be less than $N\log(N)$ [12].

The condition for breaking is also evaluated for all the intact springs. When a spring satisfies the condition for breaking, its stiffness is assigned a zero value and is removed from further calculations.

Snapshots of the tearing process taken over a wide range of values of F_{ext} reveal the existence of three distinct regimes, with critical values at F_{c1} and F_{c2}. Note that $F_{c1} < F_{c2}$. Below F_{c1}, no tearing is observed and the lattice remains intact (*intact state*). Above it, however, the lattice undergoes complete breakup (*fragmented state*) as in Fig. 4. The crack morphology of the final fragmented states is seen to vary with F_{ext}.

Intuition tells that the lattice will undergo complete breakup for *all* values of F_{ext} greater than F_{c1}, making the presence of another critical value at F_{c2} quite unexpected. The point F_{c2} is a transition from complete breakup of the lattice to partial

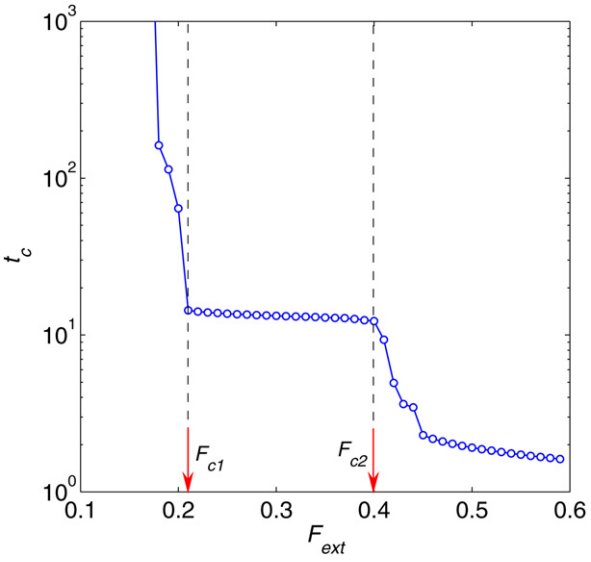

Fig. 2. Waiting time t_c as a function of applied force for an unreinforced lattice ($L = 24, l_{\max} = 1.5$). The values of the critical points F_{c1} and F_{c2} are indicated by arrows.

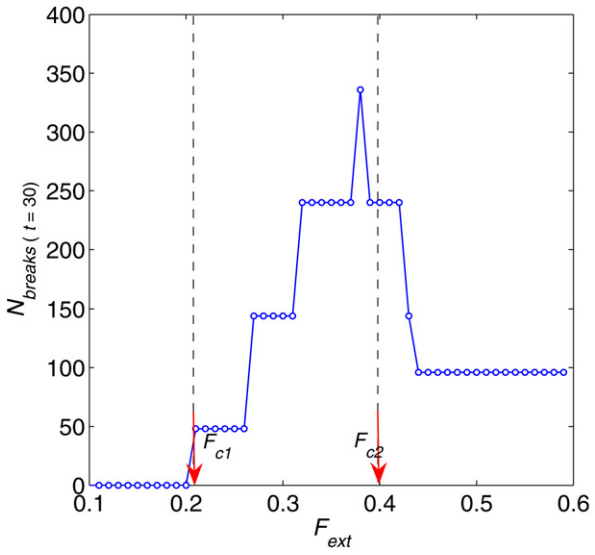

Fig. 3. Number of broken springs N_{breaks} as a function of applied force for an unreinforced lattice ($L = 24, l_{\max} = 1.5$). The values of the critical points F_{c1} and F_{c2} are indicated by arrows.

damage. Snapshots of the tearing process at $F_{\text{ext}} > F_{c2}$ regime (Fig. 5) demonstrates that only the lattice edges are ripped, leaving the rest of the lattice intact.

A more quantitative description of the tearing process as F_{ext} is increased can be obtained by monitoring the waiting time t_c and the number of broken springs N_{breaks}. The waiting time t_c, defined as the time of the first observed spring breaking, is a monotonically decreasing function of F_{ext}, as shown in Fig. 2. This indicates that increasing F_{ext} will speed up the onset or start of tearing. Note that the behavior of t_c also exhibit three regimes. At low values of F_{ext}, t_c has an infinite value, owing to the fact that no spring breaking is observed in this regime. Above F_{c1}, however, t_c assumes a finite value. The value of F_{c1} where fragmentation sets in can be identified by the location of the drop in t_c. As F_{ext} increases, there is a gradual decrease in t_c until F_{c2}, where there is another sudden drop in t_c.

To characterize the extent of tearing in the lattice N_{breaks} for different F_{ext} is monitored at time $t = 30$. As shown in Fig. 3, the behavior of N_{breaks} also shows the existence of three regimes of the tearing process. At the intact regime below F_{c1}, no spring breakings are observed. At F_{c1}, there is a sudden jump in N_{breaks}, indicating the onset of fragmentation. There is a steady increase in N_{breaks} until F_{ext} reaches the second critical value F_{c2}. At this point, there is a transition from complete breakup to partial fragmentation of the lattice, and the number of broken springs suddenly drops.

In summary, the dynamics of tearing for a uniform lattice is characterized by three regimes, with critical values at F_{c1} and F_{c2}. Below F_{c1}, the lattice is said to be in an intact state, with the dynamics characterized by an infinite waiting time and zero spring breakings. At F_{c1}, the waiting time suddenly assumes a finite value and the spring breakings becomes nonzero, indicating the transition to a fragmented state. As F_{ext} is increased, the lattice remains in a fragmented state until F_{c2}. Above this critical value, only partial fragmentation of the lattice is observed, as exhibited by the decreased number of broken springs.

4. Reinforcement strategies

The goal of structural reinforcement is to delay the onset of tearing and reduce the number of broken springs. Because of the known effects of homogeneity and disorder on the structural integrity of materials, the lattice is reinforced by varying the distribution of failure thresholds. We evaluate the waiting time t_c and number of broken springs N_{breaks} for several reinforcement strategies, and determine the failure threshold distributions (FTD) that is most successful in reinforcing the fabric.

In the computer simulations, structural reinforcement is implemented by increasing the failure thresholds of certain springs by δ, the value of which will depend on the chosen strategy. The amount of reinforcement introduced to the lattice is quantified by the reinforcement parameter α, which is defined as

$$\alpha = \frac{\sum_{\text{all springs}} l_{\max}}{\sum_{\text{all springs}} l'_{\max}} - 1, \tag{8}$$

where $l'_{\max}$ refers to the breaking thresholds after reinforcement. In essence, α is related to the ratio of the failure thresholds before and after the reinforcement; it controls the amount of reinforcement that is added to the lattice. For an unreinforced lattice, $\alpha = 0$.

In this work, two classes of reinforcement strategies are considered: (i) *dynamic*, and (ii) *static*, which are discussed below.

4.1. Dynamic strategies

Dynamic strategies are dubbed as such because they involve stretching of the lattice at some point in the process of reinforcement. Two types of dynamic strategies are considered: (a) *targeted* and (b) *adaptive*.

Targeted reinforcement is initialized by stretching a homogeneous lattice on both directions with a constant, uniform force F_{ext}. If F_{ext} is large enough, one or more springs will

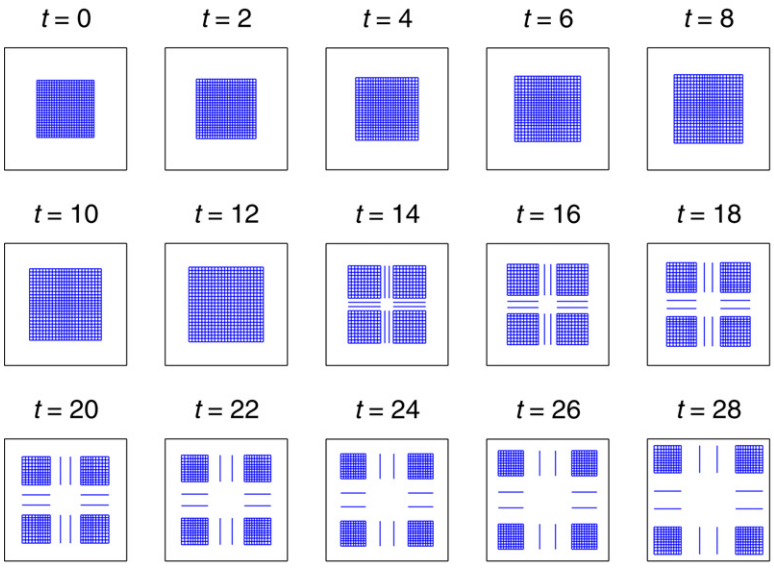

Fig. 4. Snapshots of the tearing process for an unreinforced lattice ($F_{\text{ext}} = 0.3$). The lattice is totally fragmented.

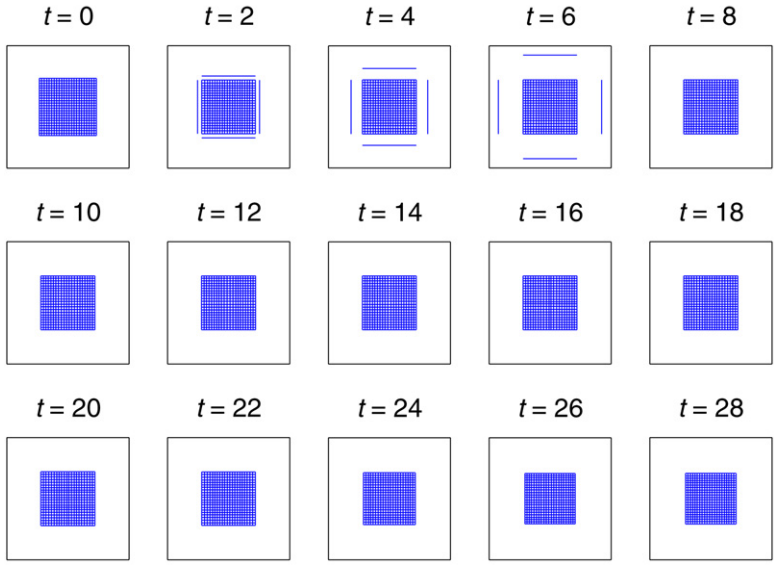

Fig. 5. Snapshots of the tearing process for an unreinforced lattice ($F_{\text{ext}} = 0.6$). Only the lattice edges are ripped, keeping the integrity of the lattice.

break after a certain waiting time t_c. As the lattice is further stretched, this initial crack will propagate through the lattice, eventually causing its fragmentation. Once the lattice has completely fragmented, stretching is halted, and the broken springs are restored to their initial stiffness. The breaking thresholds of the restored springs are then increased depending on the value of the reinforcement parameter α.

For the adaptive strategy, reinforcement is also initialized by stretching the lattice in both directions; however, at each time step, the lengths of all springs are evaluated, and the breaking threshold of the weakest springs (i.e., the springs with the greatest deformations) is increased by a small amount ϵ. The value of ϵ is chosen such that there will be no observed spring breakings as the lattice is being stretched. After $t = 300$, stretching is halted, and the breaking thresholds are normalized such that $\sum l_{\max} / \sum l'_{\max} - 1 = \alpha$.

Fig. 6 shows the resulting failure threshold distributions (FTDs) for both dynamic strategies. Notice that the reinforcements are not equally distributed among the springs; rather, they are concentrated along regions where the springs are susceptible to failure, as in the targeted case. In the adaptive case, the lattice is reinforced along the edges and at the axes of the lattice.

4.2. Static strategies

In contrast to dynamic strategies, *static* strategies do not require stretching of the lattice during the reinforcement process. Instead, reinforcements are distributed throughout the lattice based on a certain spatial distribution $\delta_{(i,j)}$. The distribution of failure thresholds after reinforcement is

$$l'^{\max}_{(i,j)-(i\pm1,j\pm1)} = l^{\max}_{(i,j)-(i\pm1,j\pm1)} + \delta_{(i,j)}, \tag{9}$$

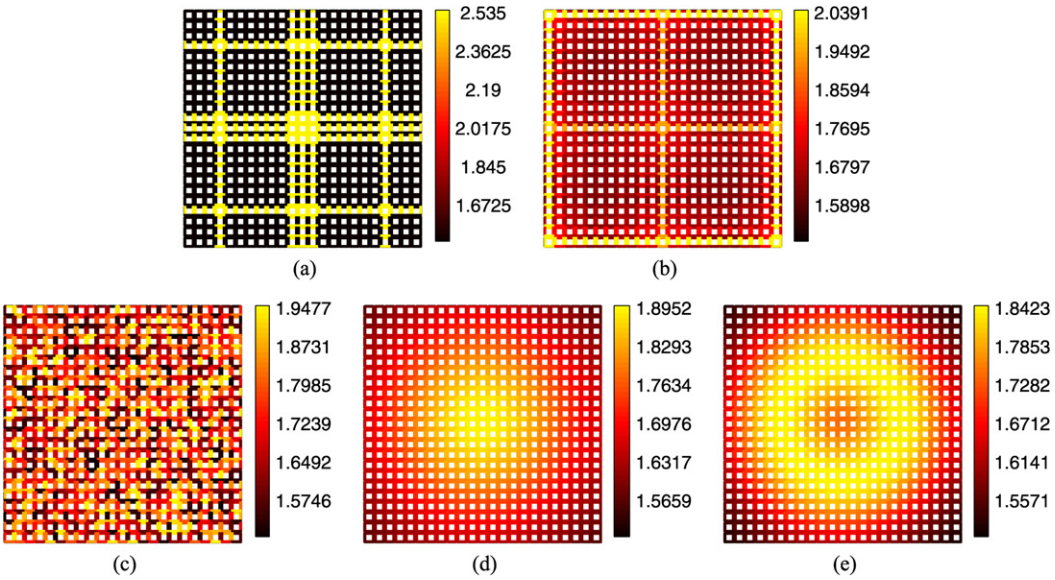

Fig. 6. Resulting failure threshold distributions for (a) targeted, (b) adaptive, (c) static random, (d) static Gaussian, (e) static toroid reinforcement, using a reinforcement parameter $\alpha = 0.15$. The values of the failure threshold varies from black (lowest) to red (intermediate) to yellow (highest). (For interpretation of the references to color in this figure legend, the reader is referred to the web version of this article.)

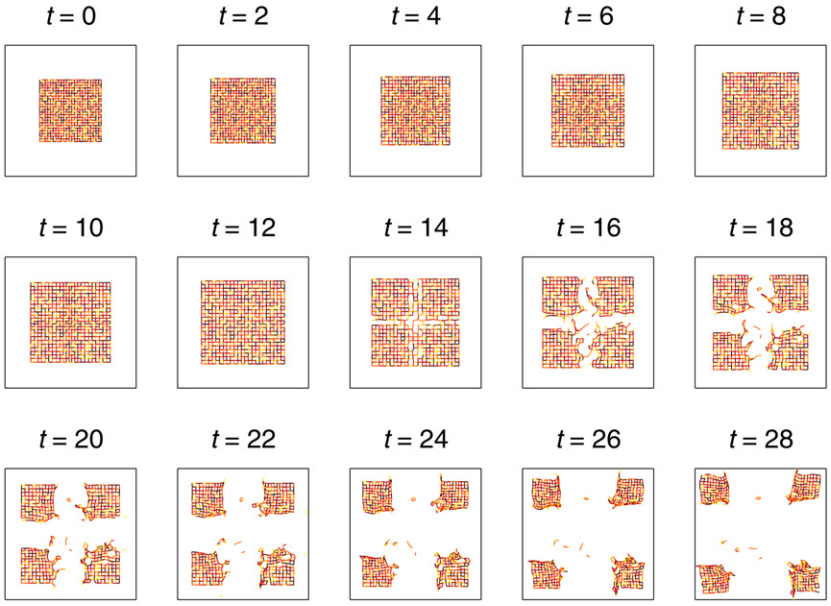

Fig. 7. Snapshots of the tearing process for a lattice with a random distribution of reinforcements ($F_{\text{ext}} = 0.35$). An animation of these snapshots can be downloaded at the author's website [13].

where $l'_{\max}$ is the threshold after reinforcement. The value of $\delta_{(i,j)}$ will depend on the chosen reinforcement strategy. In this work, three different distributions are considered: (a) *random* (Fig. 7), (b) *Gaussian* (Fig. 8), and (c) *donut-shaped* (Fig. 9). In random reinforcement, $\delta_{(i,j)}$ is a random number between 0.0 and 1.0 chosen from a uniform distribution. In Gaussian reinforcement, on the other hand, the reinforcements $\delta_{(i,j)}$ are distributed according to the spatial distribution

$$\delta_{(i,j)} \sim \exp\left\{-\left[\left(\frac{i-0.5(L+1)}{\sigma}\right)^2 + \left(\frac{j-0.5(L+1)}{\sigma}\right)^2\right]\right\}, \tag{10}$$

σ being the spread of the distribution. A smaller σ will cause the reinforcements to be concentrated at the center of the lattice. For the donut-shaped reinforcement, the corresponding distribution of reinforcements is

$$\delta_{(i,j)} \sim \exp\left\{-\left(\frac{r_{(i,j)} + 0.25(L+1)}{\sigma}\right)^2\right\} + \exp\left\{-\left(\frac{r_{(i,j)} - 0.25(L+1)}{\sigma}\right)^2\right\}, \tag{11}$$

where $r_{(i,j)} \equiv \sqrt{[i-0.5(L+1)]^2 + [j-0.5(L+1)]^2}$. In this case, σ corresponds to the radius of the donut. For all distri-

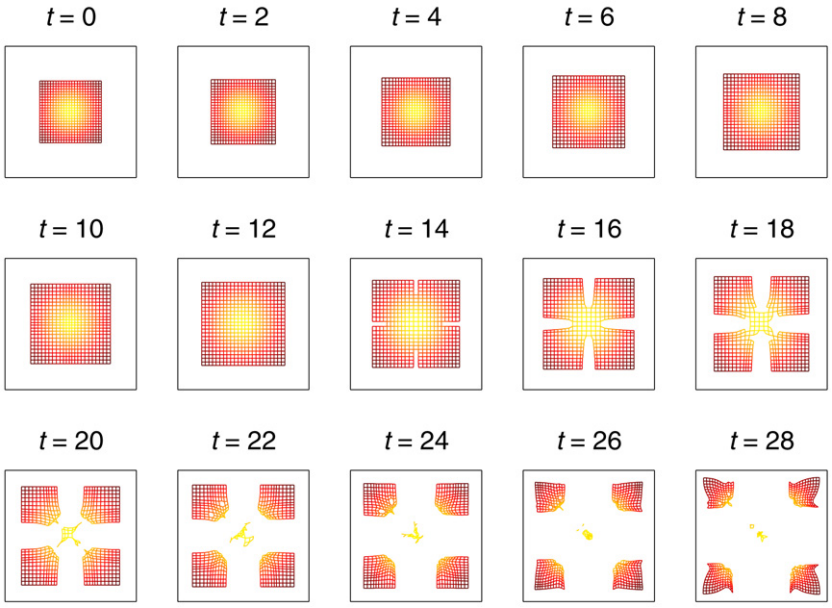

Fig. 8. Snapshots of the tearing process for a lattice with a Gaussian spatial distribution of reinforcements ($F_{\text{ext}} = 0.35$) [13].

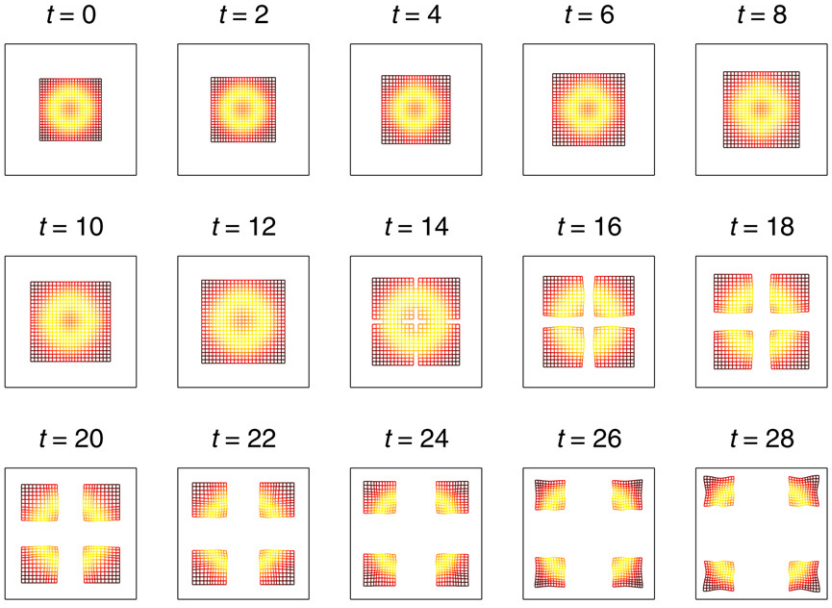

Fig. 9. Snapshots of the tearing process for a lattice with a toroidal or donut-shaped spatial distribution of reinforcements ($F_{\text{ext}} = 0.35$) [13].

butions, $\delta_{(i,j)}$ is added to the failure threshold of springs connected to node (i, j), and the new values of $l_{\max}$ are normalized depending on the chosen value of α.

4.3. Implementation

For all reinforcement strategies, simulations are performed using a lattice size $L = 24$ over a wide range of values of the parameters F_{ext} and α. Prior to reinforcement, all springs have identical failure thresholds $l_{\max} \equiv 1.5l_0$. After increasing the values of the failure thresholds based on the chosen reinforcement strategy, the lattice is stretched with an external force given by Eq. (3). The time evolution of the system is followed by solving the equations of motion given by Eq. (1), with the condition for breaking evaluated for all the intact springs at each iteration. To check if the chosen strategy is effective in reinforcing the lattice, we monitored the waiting time t_c and number of broken springs N_{breaks} as a function of F_{ext}. The lattice is said to be *reinforced* if there is (a) an increase in t_c, or (b) a decrease in N_{breaks}. Snapshots of the tearing process for the random, Gaussian, and toroid distributions are shown in Figs. 7 to 9. Notice that the FTD used has a profound effect on the tearing dynamics and the resulting crack morphology.

To quantify the success of the five strategies in reinforcing the lattice, simulations are performed varying F_{ext} in a broad range and keeping α constant. Fig. 10 shows how the waiting

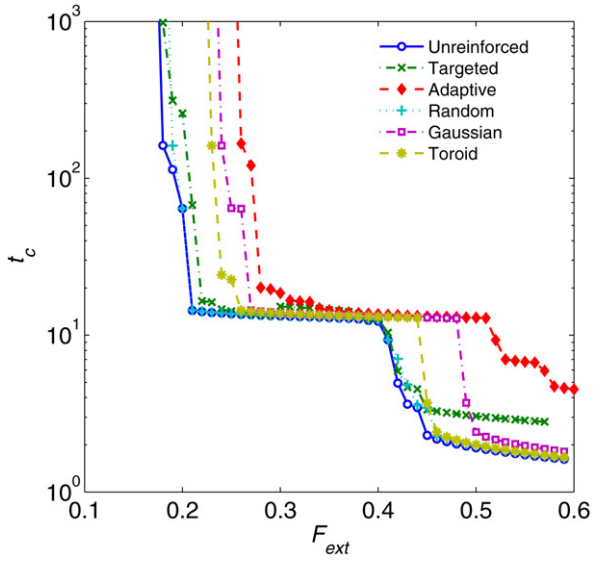

Fig. 10. Waiting time t_c as a function of the stretching force F_{ext} for the different reinforcement strategies, using $\alpha = 0.15$: unreinforced (circles); targeted (x); adaptive (diamonds); random (crosses); Gaussian (squares); toroid (stars).

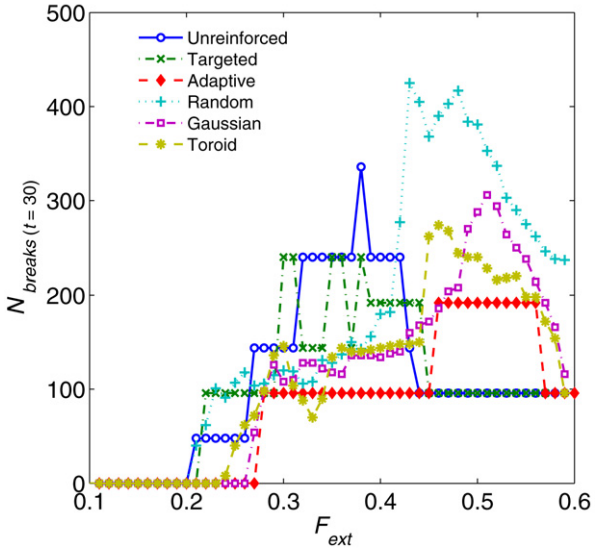

Fig. 11. Number of broken springs N_{breaks} as a function of the stretching force F_{ext} for the different reinforcement strategies, using $\alpha = 0.15$: unreinforced (circles); targeted (x); adaptive (diamonds); random (crosses); Gaussian (squares); toroid (stars).

time t_c varies with F_{ext} for each reinforcement procedure, using $\alpha = 0.15$. For all strategies, t_c is a monotonically decreasing function of F_{ext} with two sudden drops at the critical forces F_{c1} and F_{c2}. However, the values of F_{c1} and F_{c2} are shifted to the right as compared to the unreinforced case. Because F_{c1} marks the transition from the intact phase to the fragmentation phase, the observed shift in F_{c1} indicates a delay in the onset of fragmentation. A comparison of the five strategies reveal that the adaptive strategy caused the greatest shift in F_{c1}, followed closely by the Gaussian and toroidal strategies. Interestingly, there is no significant increase in F_{c1} for the targeted case, suggesting that reinforcing the lattice along its weak spots does not necessarily make the lattice stronger. Also, a random distribution of reinforcements does not significantly strengthen the lattice.

More insight into the fragmentation process can be obtained by looking at the number of broken springs N_{breaks} as a function of the stretching force. As shown in Fig. 11, all strategies are able to decrease the number of broken springs for values of F_{ext} less than ≈ 0.4. Above this value, however, N_{breaks} is greater than that for the unreinforced case, rendering all strategies to be ineffective in this region. The reduction in N_{breaks} in the region $F_{\text{ext}} \lessapprox 0.4$ is most evident for the adaptive case, followed by the Gaussian and toroid distributions. Interestingly, the random and targeted procedures are also able to decrease N_{breaks} by a significant degree, even if they are ineffective in delaying t_c.

Fig. 12 shows the effect of increasing the reinforcement parameter α on t_c. In the graphs, the arrows indicate the direction of increasing α. For all strategies, an increase in α causes the plot of t_c versus F_{ext} to shift to the right, leading to the increase of F_{c1}. The increase of F_{c1} with α is most notable for the adaptive, Gaussian, and toroid cases. For the targeted and random cases, the change is barely perceptible. Also, the number of broken springs N_{breaks} decreases with α for F_{ext} less than ≈ 0.4, as shown in Fig. 13. For $F_{\text{ext}} \gtrapprox 0.4$, the reinforcement fails and the number of broken springs increases as compared to the unreinforced case.

For the Gaussian and toroid procedures, the parameter σ also affects the efficacy of reinforcement. It can be seen in Figs. 14 and 15 that σ has the same effect as α. As σ is increased, the plot of t_c versus F_{ext} is translated to the right. Consequently, the critical value F_{c1} needed to achieve fragmentation increases. Also, N_{breaks} decreases with σ for F_{ext} less than ≈ 0.4. Above it, the reinforcement fails and the number of broken springs increases as compared to the unreinforced case.

5. Lattice size sensitivity

The dependence of our results on the lattice size is investigated by extensively performing numerical experiments for the case of $N = 12$, 24, 50, 80 and 100. All configuration types (unreinforced and reinforced) are observed to follow similar behavior as N is increased, hence any representative procedure will suffice in describing the lattice sensitivity of the model.

Fig. 16(a) shows that for the case of Gaussian-reinforced lattice, the general trend of t_c against F_{ext} is preserved as N is increased. Further, the location of the transition points F_{c1} and F_{c2} is generally intact and independent of N (compare to Fig. 10). For F_{ext} between the transition points F_{c1} and F_{c2} ($0.3 \leqslant F_{\text{ext}} \leqslant 0.45$), t_c is seen to increase linearly with N, while the waiting time elsewhere is observed to be N-independent. For instance, for $F_{\text{ext}} < F_{c1}$ almost no breaking occurs, but when $F_{\text{ext}} > F_{c2}$ immediate fragmentation happens. The linear dependence of t_c with N is expected since t_c is inversely proportional to the force between nodes ($t_c \sim 1/F_{\text{node}}$) and for any N: $\langle F_{\text{node}} \rangle = 4NF_{\text{ext}}/N^2 = 4NF_{\text{ext}}$. The implemented biaxial stretching condition uniformly distributes the effect of F_{ext} in the square lattice. Imposing symmetry arguments, it follows that $t_c \sim N$.

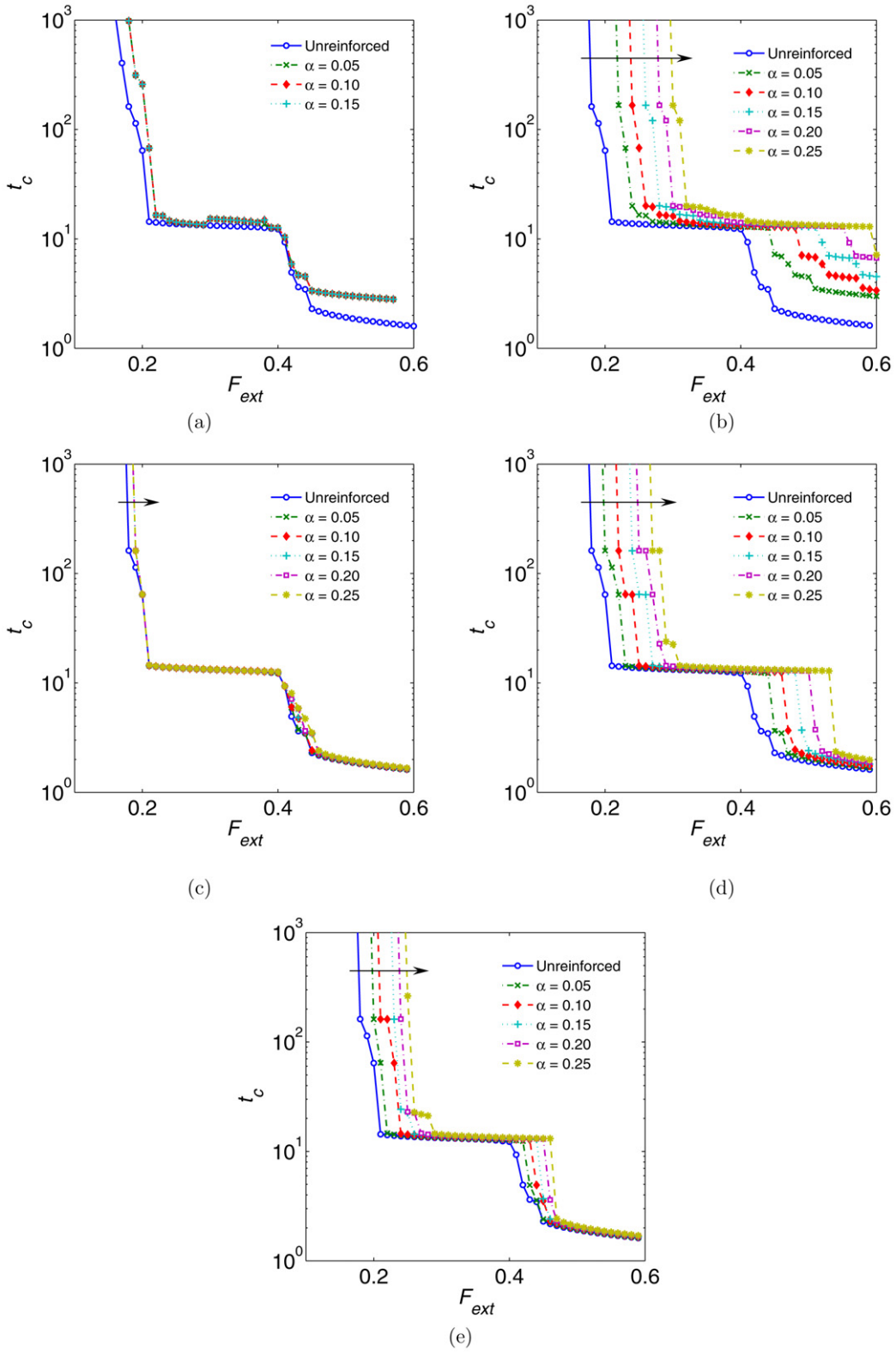

Fig. 12. Effect of the reinforcement parameter α on the waiting time t_c for the different reinforcement strategies: (a) targeted, (b) adaptive, (c) random, (d) Gaussian, (e) toroid. Arrows indicate the direction of increasing α. The critical value F_{c1} need to achieve fragmentation increases with α, implying a delay in the onset of fragmentation.

As expected, the dynamical dependence of N_{breaks} with F_{ext} for any time t follows the linear dependence of t_c with N. That is, the instantaneous state at time t of an $N \times N$ lattice directly *corresponds* to the state evolved by an $\varrho N \times \varrho N$ after ϱt, where ϱ is a lattice size scaling parameter. The trend similarity of the plot of N_{breaks} against F_{ext} for

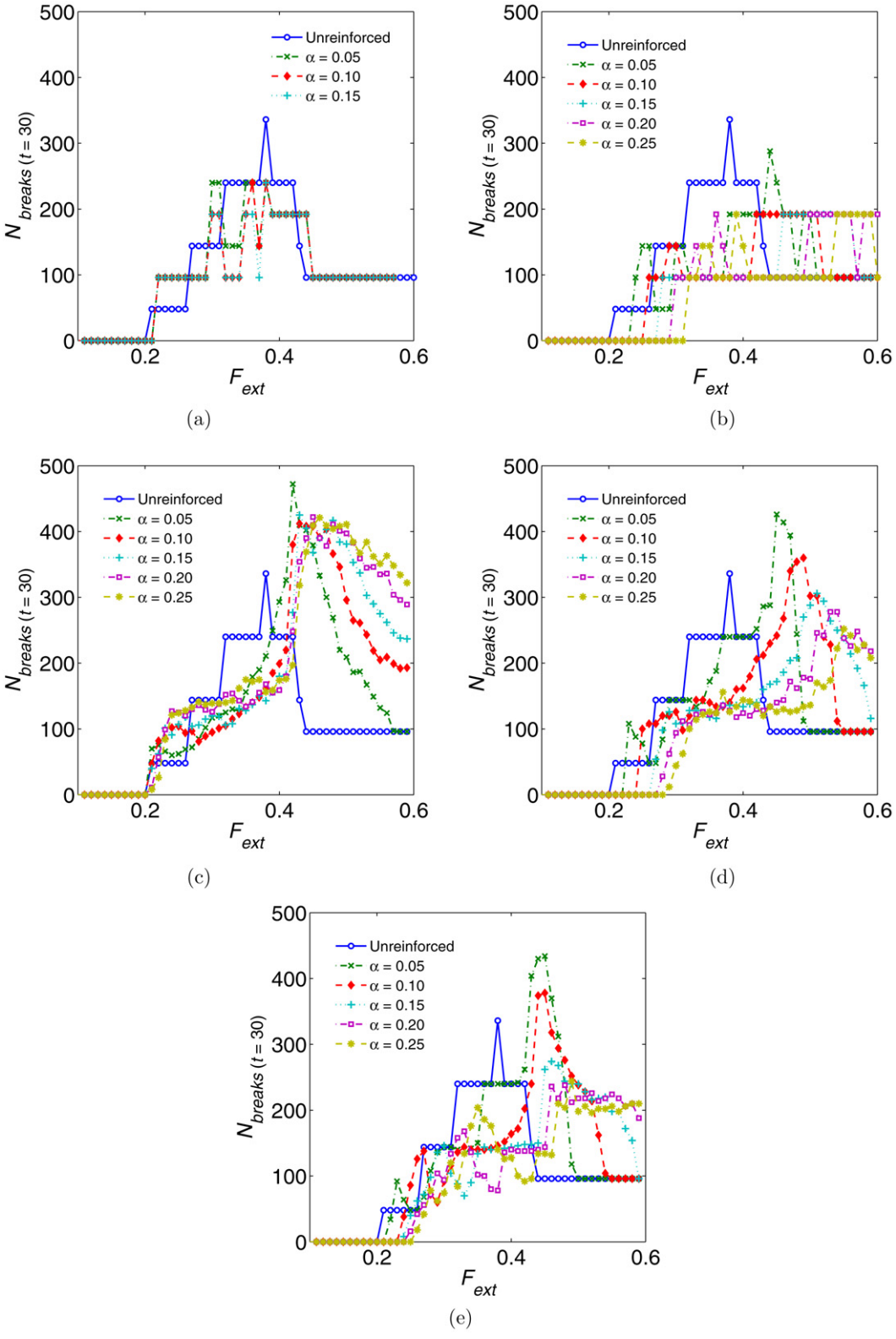

Fig. 13. Effect of the reinforcement parameter α on the number of broken springs N_{breaks} for the different reinforcement strategies: (a) targeted, (b) adaptive, (c) random, (d) Gaussian, (e) toroid. For all strategies, the number of broken springs decreases with α for $F_{\text{ext}} \lessapprox 0.4$.

different N but at *corresponding times* is demonstrated in Fig. 16(b). Easily noticeable is the alignment of the maxima N_{breaks} ($F_{\text{ext}} = 0.3, 0.5$) and minimum N_{breaks} ($F_{\text{ext}} = 0.4$) for different N. As shown in the inset of Fig. 16(b), N_{breaks} for *corresponding times* linearly increases with N^2. Such is anticipated because N_{breaks} increases proportional to the number of lattice nodes, which in turn grows proportional to N^2.

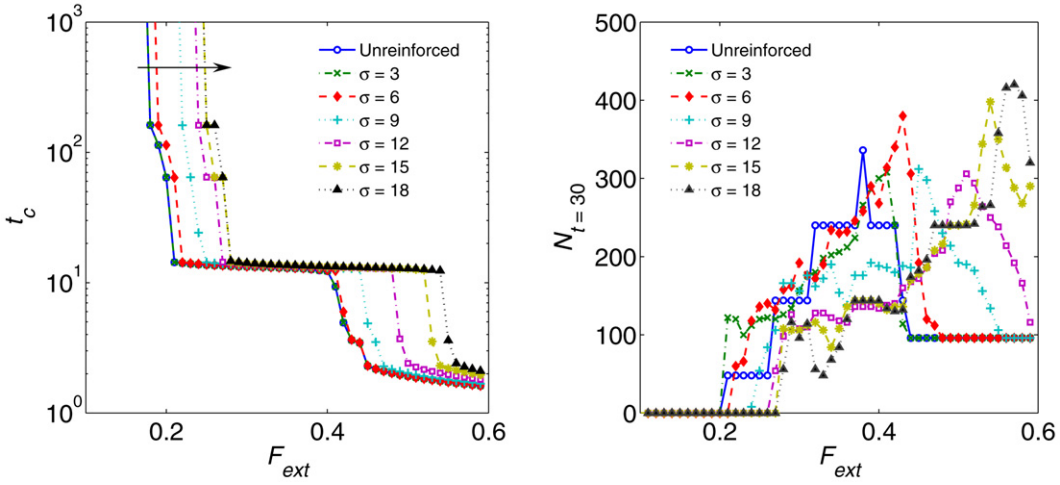

Fig. 14. Waiting time t_c and number of broken springs N_{breaks} at $t = 30$ as a function of the stretching force F_{ext} for different values of σ (Gaussian). Arrow indicates the direction of increasing σ.

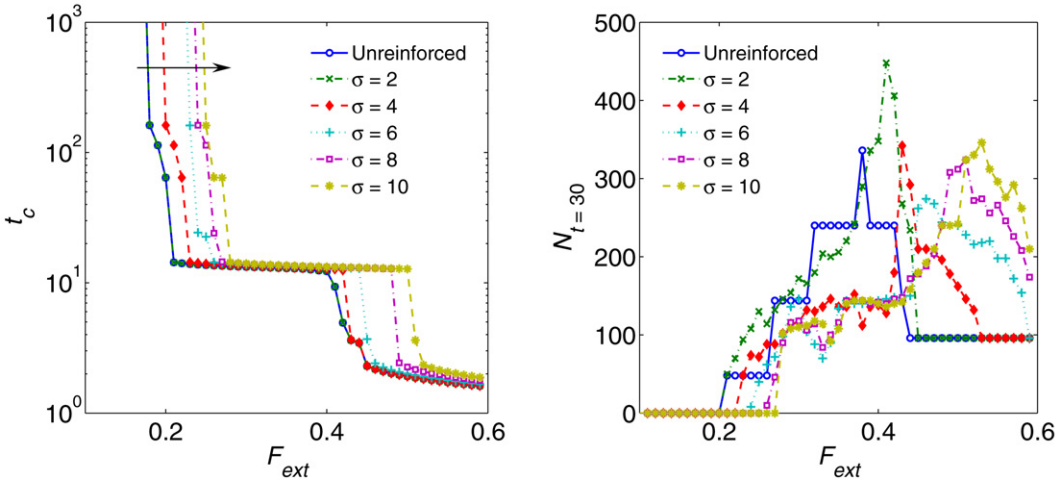

Fig. 15. Waiting time t_c and number of broken springs N_{breaks} at $t = 30$ as a function of the stretching force F_{ext} for different values of σ (toroid). Arrow indicates the direction of increasing σ.

There is no assurance that the system will achieve static equilibrium, and therefore the more meaningful parameter is the state behavior at an instantaneous time. As a case in point, for weak forces ($F_{\text{ext}} < 0.2$ in our model) breaking do not typically occur and therefore the system tends to be in dynamic equilibrium (oscillates between different states), instead of proceeding to a static state. The framework of *corresponding times* described above allows comparison of the temporal evolution of systems with different lattice sizes.

6. Related ideas and conclusion

The use of lattice models as exemplified here is relevant to the design of stronger materials and optimization of structural composition. The procedure provides a valid alternative to FEA, especially in cases when structural disorder and inhomogeneities are particularly strong [2]. In textile research, for example, the design of woven fabrics is influenced by parameters such as the raw material of the warp and the weft, the linear density of the warp and weft, the warp and weft setting, and fabric weave [14]. Designing fabric that gives the greatest resistance to tearing without sacrificing comfort can be implemented by the introduction of randomness or disorder. It has been known that inhomogeneities in a material has profound effects on its strength, since fracture typically starts from weaker spots such as preexisting cracks or voids [2]. If the dynamic make-up of such fabric is similar to the system we discussed here, then the evolution of stress and strain of various weaving patterns can be correspondingly predicted.

Straightforward description of elasticity and disorder of surface fractures is the main advantage of our model in characterizing fragmentation process. The elastic medium is aptly represented by a network of springs, while the disorder is modeled either by assigning random failure threshold on the springs or by removing a fraction of the links. Upon imposing appropriate boundary conditions, the fracture process is easily tractable for an arbitrary time step.

In conclusion, a general method for characterizing the fracture propagation of an elastic sheet based on a lattice model is implemented. The procedure allows testing of arbitrary

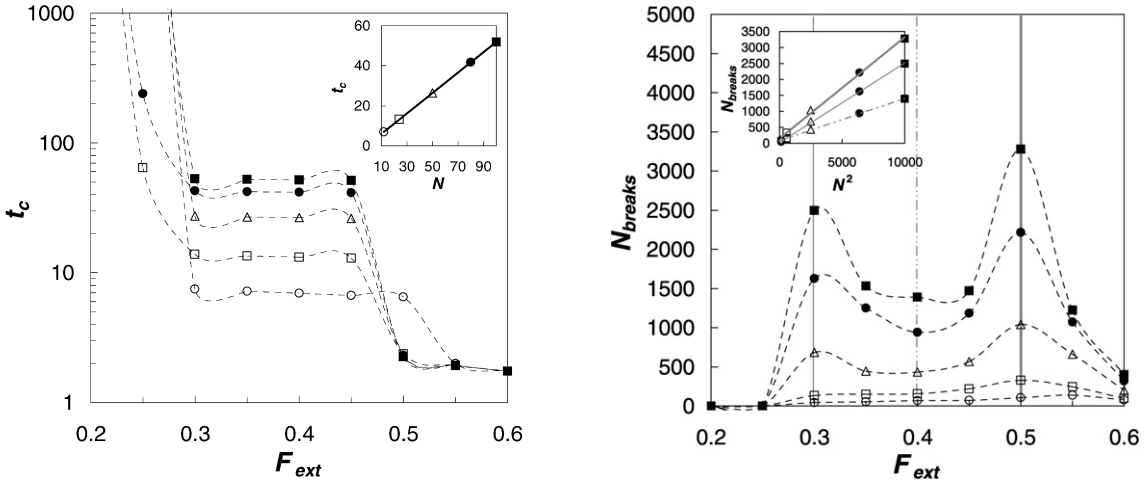

(a) (b)

Fig. 16. Dependence of (a) Waiting time t_c and (b) number of broken springs N_{breaks}, for different stretching force F_{ext} at various lattice sizes $N = 12$ (○), 24 (□), 50 (△), 80 (●) and 100 (■) in a Gaussian-reinforced lattice. Inset of (a) shows the linear dependence of t_c with N (fitted line: $t_c = 0.51N + 0.9$ with $R^2 = 1.0$). Inset of (b) shows the linear dependence of N_{breaks} with N^2 for $F_{\text{ext}} = 0.3, 0.4, 0.5$ (fitted lines from top: $N_{\text{breaks}} = 0.31N^2 + 208.42$, $N_{\text{breaks}} = 0.253N^2 + 17.50$, $N_{\text{breaks}} = 0.13N^2 + 76.42$; $R^2 = 1.0$ for all). The *corresponding times* for $N = \{12, 24, 50, 80, 100\}$ are respectively $t = \{18, 36, 75, 120, 150\}$. Similar are observed for all other configurations (unreinforced and reinforced).

load distribution and disparate reinforcement protocols. The Gaussian and adaptive procedures are most effective in delaying the onset of tear propagation, as shown by the increase in t_c, and the increase in the value of the critical force F_{c1} needed to achieve fragmentation. However, the Gaussian procedure is more efficient than the adaptive procedure because it requires less computation time.

Acknowledgement

The authors would like to thank the Computational Science Research Center of the University of the Philippines for the use of their High Performance Computing Facility. Useful insights from Dr. Giovanni Tapang are also appreciated. G.A. Esleta is also grateful to the financial assistance of the Department of Science and Technology.

References

[1] J.B. Rundle, W. Klein, Phys. Rev. Lett. 63 (1989) 171.
[2] M.J. Alava, P.K. Nukala, S. Zapperi, Adv. Phys. 55 (2006) 3.
[3] L. de Arcangelis, S. Redner, H.J. Herrmann, J. Phys. (Paris) Lett. 46 (1985) 583.
[4] R. Burridge, L. Knopoff, Bull. Seis. Soc. Amer. 57 (1967) 341.
[5] K. Chen, P. Bak, S.P. Obukhov, Phys. Rev. A 43 (1991) 2.
[6] K.-t. Leung, J. Müller, J.V. Andersen, J. Phys. I France 7 (1997).
[7] J.V. Andersen, Y. Brechet, H.J. Jensen, Europhys. Lett. 26 (1994) 13; J.V. Andersen, Phys. Rev. B 49 (1994) 9981.
[8] K.-t. Leung, J.V. Andersen, Euro. Phys. Lett. 38 (1997) 8.
[9] F.K. Wittel, F. Kun, H.J. Herrmann, B.H. Kröplin, Phys. Rev. Lett. 93 (2004) 3; F.K. Wittel, F. Kun, H.J. Herrmann, B.H. Kröplin, Phys. Rev. E 71 (2005) 016108.
[10] Z. Olami, J.S. Feder, K. Christensen, Phys. Rev. Lett. 68 (1992) 1244; K. Christensen, Z. Olami, Phys. Rev. A 45 (1992) 665.
[11] P. Henrici, in: Discrete Variable Methods in Ordinary Differential Equations, John Wiley & Sons, 1967, p. 123.
[12] C. Monterola, C. Saloma, Phys. Rev. Lett. 86 (2001) 4741; C. Monterola, C. Saloma, Phys. Rev. E. Rap. Comm. 57 (1998) 1247.
[13] Supplementary materials available at: http://www.nip.upd.edu.ph/ipl/mem/homepages/cmonterola/.
[14] E. Kumpikaitė, A. Sviderskytė, Mater. Sci. 12 (2006) 2.